

PIV Measurements of Free-falling Irregular Particles

by

C. Losenno⁽¹⁾ and W.J. Easson⁽²⁾

School of Mechanical Engineering
The University of Edinburgh
The King's Buildings
Edinburgh EH9 3JL, Scotland, UK
E-Mail¹: c.loosenno@ed.ac.uk
E-Mail²: bill.easson@ed.ac.uk

ABSTRACT

The terminal velocity of irregular particles in a free-falling stream has been measured experimentally by using Particle Image Velocimetry. The aim of the measurements was to assess the influence of particle shape on the particle dynamics and compare the results with spherical particles. Measurements were carried out by using coarse glass powder and spherical glass beads of the same density and similar size distribution. Particle diameters ranged from 150 μm to 180 μm . Measurements were taken at both the developing region and self-similar region of the particles stream, as shown in figure 1.

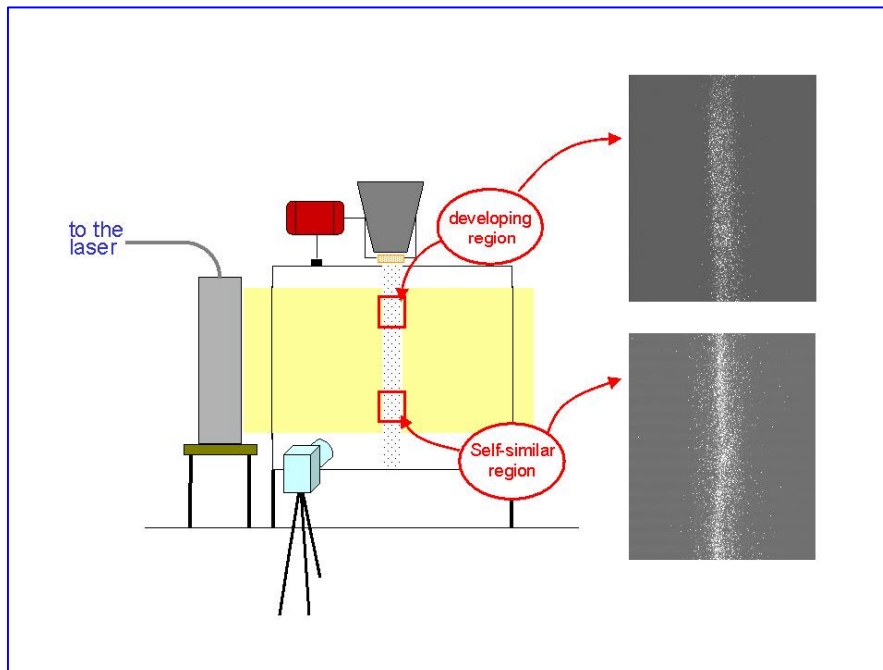


Fig. 1. Experimental set-up and measurements locations

Detailed particle velocity information for both spherical and irregular particles were obtained. Significant differences between the behaviour of spherical and irregular particles were observed at both stream locations. Terminal velocity of irregular particles has been found to be smaller than the velocity of spherical particles at all the measurement points.

The experimental results have been compared to empirical data. The drag coefficient of irregular particles has been found to be higher than both the predicted and experimental drag coefficient of spherical particles. The sphericity of irregular particles was found to be equal to 0.6.

1. INTRODUCTION

Multiphase flows are encountered in numerous engineering applications. The typical fluid is usually a gas carrying particles, either solid or liquid. When the particles are solid the flow is referred to as a gas-solid flow. Often in these flows various particle-particle interactions, such as collisions and coalescence, can be neglected and the flow is referred to as dilute two-phase flow. Examples of such flows are pollutant spread from stack emissions, food processing, pneumatic transport of powdered material, pulverised coal combustion, cyclone separators and classifiers, and can be found in the chemical, pharmaceutical, cement and power industry. Accurate computational modelling of gas-solid flow is essential for the optimum design and characterisation of these systems.

The forces acting on a single particle have been identified (Clift et al., 1978). Many experimental works have been carried out in order to determine the drag coefficient and/or the velocity of particles in a gas-solid flow. The bulk of research effort has been directed mainly at spherical particles and in some cases at regular non-spherical particles, due to the obvious advantages both in experimental and numerical studies.

Experiments have been performed by McKay et al. (1988) for disks and cylinders, Sharma and Chhabra (1991) for cones, Lasso and Widman (1986) for hollow cylinders, Hartamn et al. (1994) for limestone and lime glass spheres, and Chhabra et al. (1996) for disks and square plates. Correlations able to predict the drag coefficient for particles of various shapes have been formulated on the basis of the experimental data available in the literature. These include Turton and Clark (1987), Haider and Levenspiel (1989), Swamee and Ojha (1991), Ganser (1993), and Hartman et al. (1994).

These results serve as a useful basis to characterise and predict the behaviour of particle-laden flows. However, there is still a lack of accurate experimental data on non-spherical and irregular particles in the literature for validating multiphase flows. To address this need, experiments were carried out to collect detailed information on irregular particles in a free falling stream, and assess the influence of particle shape on the flow dynamics.

2. EXPERIMENTAL SET-UP

The particles used in the present experiments were glass beads and crushed glass ($\rho=2590 \text{ kg/m}^3$). Figure 2 shows microscope photographs of both spherical and irregular particles.

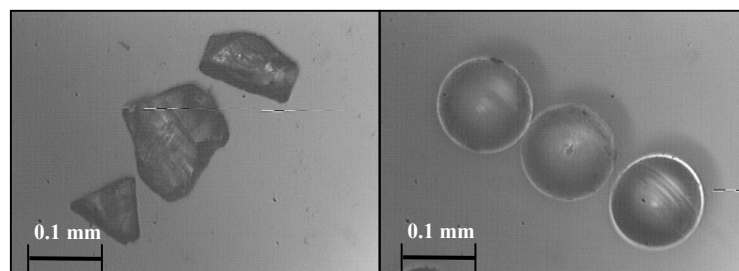


Figure 2. Microscope photographs of irregular and spherical particles

Particle diameter ranged from 150 to 180 μm . Both spherical and irregular particles have been sized by using test sieves (Endecotts Brass S/Steel mesh) of corresponding apertures. The particle distribution is shown in figure 3.

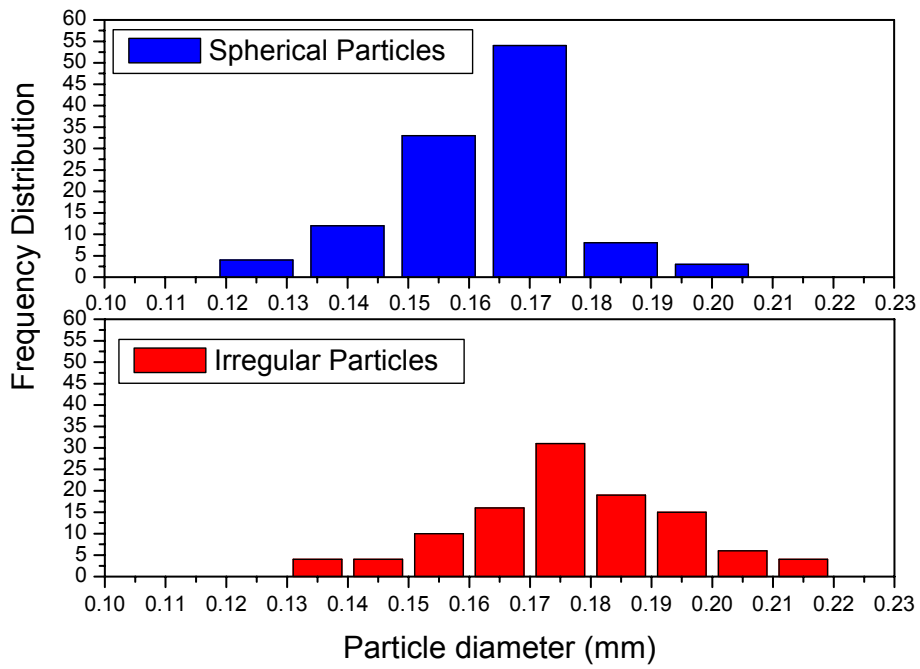


Fig. 3. Size distribution of spherical and irregular particles

The set-up used for the experiments is shown in figure 4.

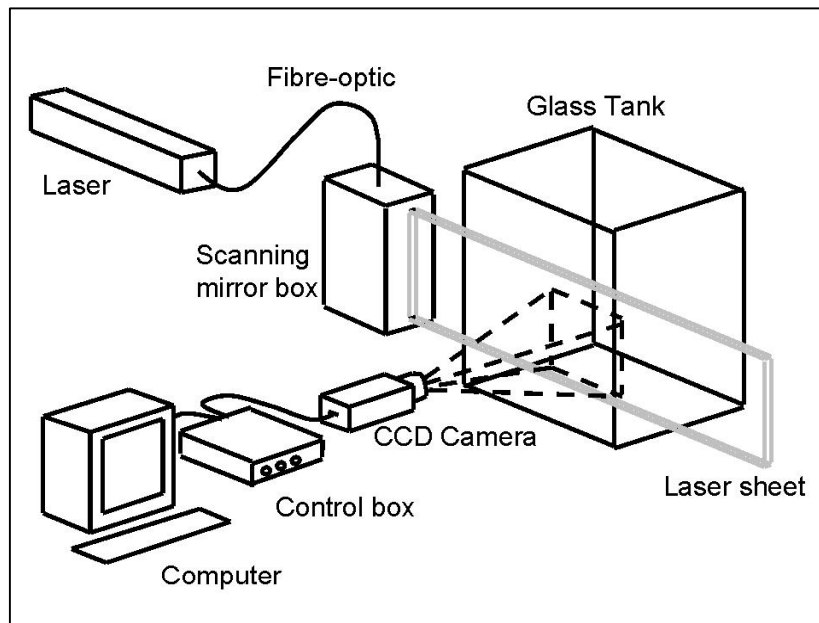


Fig. 4. Experimental set-up

The powder stream was confined in a glass tank. In order to avoid wall effects, a large tank 1m x 1m x 1m was used. The particles were stored in a hopper mounted directly above the tank. A vibrating mechanism connected to the hopper ensured an even particle flow rate. In order to obtain an even distribution of particles, a mesh at the base of the hopper was introduced. The mesh was carefully selected for each particle diameter range and shape in pre-performed tests. The particle mass flow rate from the hopper was controlled by an iris, which allowed the diameter to be varied from 1.5 to 3 mm. The aperture of the orifice was changed systematically until a similar mass flow rate of 0.3 g/s was achieved for spherical and irregular particles in both measurement areas. Particles flow from the hopper to the tank through the mesh and were collected in the receiving tank.

Particle Image Velocimetry (PIV) was used to measure the velocity of the particles in the free falling stream. A single-frame/multi-pulse technique was used. A 15W Spectra-Physics 171 Argon-Ion laser was used to produce a laser light sheet. The laser beam was directed to the experimental set-up through a fibre optic. A scanning beam method with a scan interval of 5ms was used to illuminate the flow and a 1Mb Kodak Megaplug CCD camera recorded the images.

The PIV image sequence was transferred to a DANTEC PIV 2000 Processor to produce vector maps. Auto-correlation was used for the experiments reported in this paper. Initial and final particle positions were recorded on the same camera frame, and the recorded image was then correlated with spatially shifted versions of itself. In order to improve the signal-to noise ratio, three consecutive light-sheet pulses were recorded in the same camera frame. Interrogation areas equal to 64x128 pixels were used for both spherical and irregular particles.

Incorrect velocity vectors resulting from noise peaks in the correlation function were eliminated by using peak height validation and range validation. No further filtering technique was applied.

3. RESULTS

Smooth discharge was achieved for the chosen orifice and mesh sizes during the measurements. Figure 5 shows the time history of the measured particle velocity at the centre of the powder stream for both developing and self-similar region.

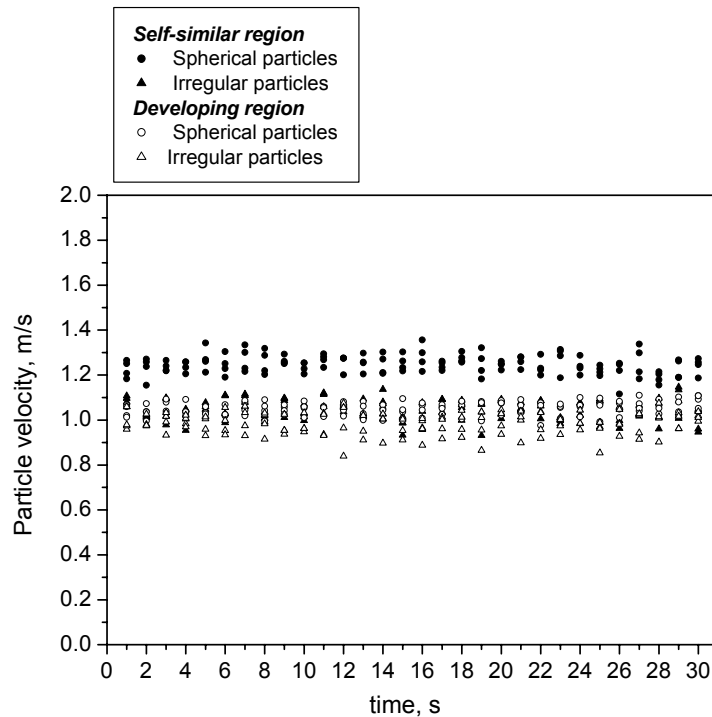


Fig. 5. Time history of measured particle velocity at the centre of the powder stream

In all experimental conditions, the minimum, maximum and mean terminal velocity of spherical particles was observed to be higher than the velocities of irregular particles. The mean, minimum and maximum velocities also increased in the self-similar region of the stream. An overview of the velocity values is shown in figure 6.

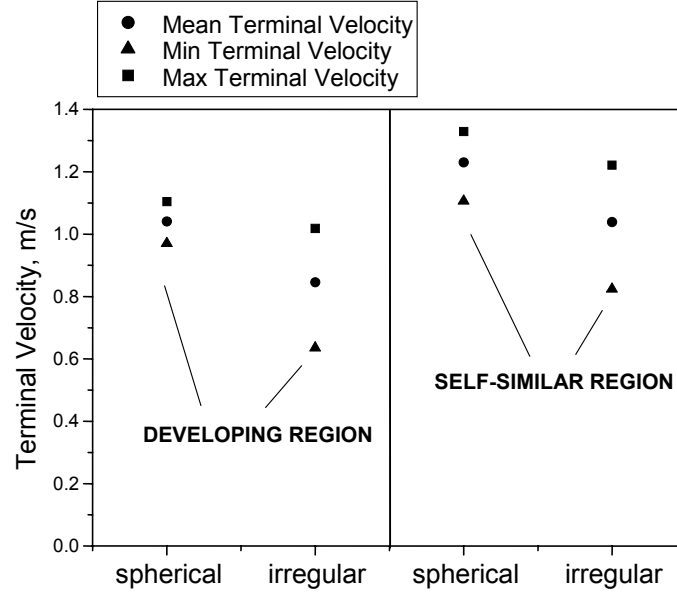


Figure 6. Mean, maximum and minimum velocity of spherical and irregular particles in the developing region and self-similar region

For both spherical and irregular particles, 30 PIV images were recorded in a sampling time of 30 seconds. The velocity data obtained by the image post-processing was then averaged over the 30 images. The velocity at every single location of the control area is therefore given by:

$$\bar{u} = \frac{1}{N} \sum_{i=1}^N u_i \quad (1)$$

where u_i represents a sample velocity at the measuring point and N is the number of samples. This yielded an “averaged velocity map” for each flow, to which the results presented in the following refer.

The fluctuation velocity has been calculated as the root-mean-square of the average of the squared difference between the local velocity at the measuring point and the mean velocity at the same point:

$$\sqrt{u'^2} = \sqrt{\frac{1}{N} \sum_{i=1}^N (u_i - \bar{u})^2} \quad (2)$$

where \bar{u} is the local mean velocity as defined by equation 1.

Results are presented for both spherical and irregular particles. For spherical particles, the terminal velocities lay between 1 and 1.1 m/s in the developing region and between 1.1 and 1.4 m/s in the self-similar region. In the case of irregular particles, terminal velocity varied between 0.6 and 1 m/s in the developing region and between 0.7 and 1.2 m/s in the self-similar region. The radial profiles of the mean terminal velocity and fluctuation velocity of spherical and irregular particles are shown in figure 7.

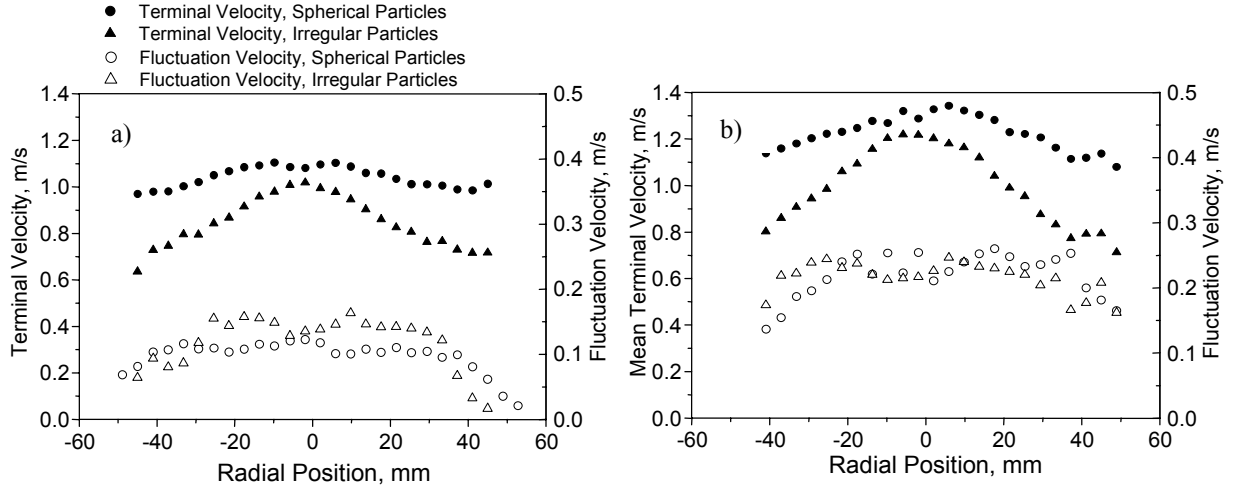


Fig. 7. Radial profile of mean terminal velocity and fluctuation velocity of spherical and irregular particles a) at the developing region and b) the self-similar region.

The velocity profiles are clearly distinguishable. Irregular particles show a consistently lower velocity than spherical particles. In the developing region, the profile of spherical particles appears to be more even across the stream compared to the irregular particles, which maintain a distinct velocity peak at the jet centreline. The difference between velocities at the flow edges and centreline becomes more evident in the self-similar region, where the particles have all reached their terminal velocity. Figure 4b shows that the difference between the velocity at the flow centreline and the flow edges increases as the particles move towards the self-similar region. This is particularly true for the irregular particles, whereas the spherical particles maintain a flatter radial profile. The fluctuation velocities appear to increase significantly moving from the developing to the self-similar region and stabilise at about 0.25 m/s for both spherical and irregular particles.

The experimental data can be compared with empirical correlations for predicting the terminal velocity of free falling particles. For spherical particles, the correlation given by Haider and Levenspiel (1989) is:

$$u_* = \left(\frac{4 \text{Re}}{3 C_D} \right)^{\frac{1}{3}} = v_t \left[\frac{\rho_f^2}{g\mu(\rho_s - \rho_f)} \right]^{\frac{1}{3}} \quad (3)$$

$$d_* = \left(\frac{3}{4} C_D \text{Re}^2 \right)^{\frac{1}{3}} = d \left[\frac{g\rho_f(\rho_s - \rho_f)}{\mu^2} \right]^{\frac{1}{3}} \quad (4)$$

$$u_* = \left[\frac{18}{d_*^2} + \frac{(0.5909)}{d_*^{0.5}} \right]^{-1} \quad (5)$$

$$C_D = \frac{24}{\text{Re}} (1 + 0.1806 \text{Re}^{0.6459}) + \frac{0.4251}{1 + \frac{6880.95}{\text{Re}}} \quad (6)$$

where u_* and d_* are dimensionless velocity and diameter, respectively, ρ_f the fluid density and ρ_s the particle density.

According to Haider and Levenspiel (1989), the following equation can be used to predict quite accurately the drag coefficient of non-spherical particles:

$$C_D = \frac{24}{\text{Re}} \left[1 + (8.1716 \exp(-4.0655\Phi)) \right] \text{Re}^{0.0964+0.5565\Phi} + \frac{73.69 \text{Re} \exp(-5.748\Phi)}{\text{Re} + 5.378 \exp(6.2122\Phi)} \quad (7)$$

The particle drag coefficient and Reynolds number have been calculated by using the following equations:

$$C_D = \frac{4}{3} \frac{gd(\rho_s - \rho_f)}{u^2 \rho_f} \quad (8)$$

$$\text{Re} = \frac{du\rho_f}{\mu} \quad (9)$$

Figure 8 shows the comparison between the drag coefficient as determined from the present experimental results and the empirical correlation of Haider and Levenspiel (1989).

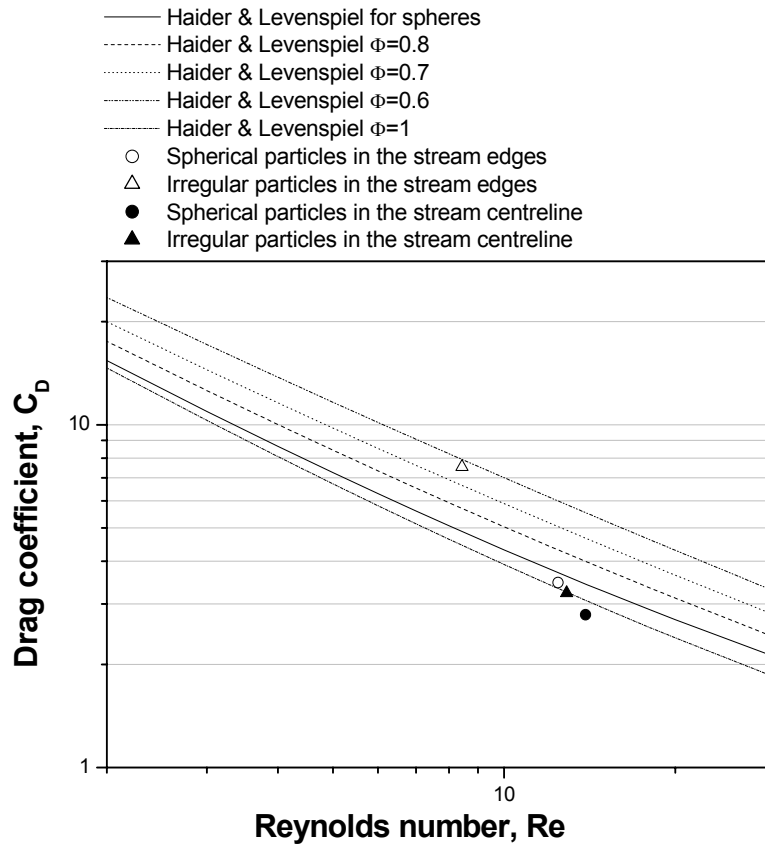


Fig. 8. Comparison between empirical and experimental drag coefficient in the self-similar region

The empirical results for particles having sphericity $\Phi=1$ to 0.6 have been reported in figure 8, as well as the empirical results for spheres. As shown in the figure, the drag coefficient of spherical particles in the centreline is below the line for spheres. This is due to the augmentation of particle velocity caused by wake effect of the particle

stream. The drag of irregular particles lies on the line $\Phi \cong 1$, suggesting that, although irregular particles do experience a slightly higher drag coefficient, they behave as the spherical particles in the stream centreline. In the stream edges, the particle flow is more disperse and the wake effect is reduced. Here particle behaviour approaches the dynamics of unbounded particles. The drag coefficient of irregular particles is significantly higher than the drag of spherical particles. The drag coefficient lies on the curve for $\Phi \cong 0.6$.

4. CONCLUSIONS

The terminal velocities of irregular and spherical particles in a free falling stream have been measured experimentally in the developing region and in the self-similar region. Experiments were performed using a Particle Image Velocimetry technique. Data presented includes profiles of mean velocity and fluctuation velocity. Experimental measurements showed that significant differences in the velocity profiles occur due to particle shape. In the developing region, the velocity of irregular particles showed a distinct peak in the centreline of the flow, whilst spherical particles exhibits a nearly flat radial profile. In the self-similar region, the terminal velocity of spherical particles evolves into a more pronounced profile with higher values in the jet centreline. However the biggest difference between velocity at the flow edges and centreline was found for irregular particles.

The experimental data is in good agreement with the empirical correlations of Haider and Levenspiel. In the stream centreline, the drag coefficient of irregular particles approached the drag of spherical particles. In the jet edges, the observed dynamic behaviour of the particles in the stream moved towards the one of unbounded particles. The drag coefficient of irregular particles nearly doubled the drag of spherical particles at the stream edges and equalled the empirical drag coefficient for sphericity $\Phi=0.6$.

REFERENCES

Chhabra R. P., Andrew McKay and Peter Wong (1996) Drag on discs and square plates in pseudo-plastic polymer solutions, *Chemical Engineering Science*, 51, 5353-5356

Clift R., J. Grace and M.E. Weber (1978). *Bubbles, Drops and Particles*. Academic Press, New York, U.S.A.

Haider A. and O. Levenspiel (1989). Drag coefficient and Terminal velocity of spherical and non-spherical particles. *Powder technology* 58, 63-70

Hartamn M., O. Trnka, K. Svoboda (1994) Free settling of non-spherical particles *Industrial & Engineering Chemistry Research*. 33, 1979-1983

Lasso I. A. and P. D. Weidman (1986). Stokes drag on hollow cylinders and conglomerates. *Physics of Fluids* 29, 3921-3934

Leibster H. (1927). *Ann.Physik*, 4(82), 341

McKay G., W.R. Murphy, M. Hillis (1988). Settling characteristics of disks and cylinders. *Chem. Eng. Res. Des.* 66(107), 107-112

Sharma M.K., Chhabra, R.P., 1991. An experimental study of free fall of cones in Newtonian and Non-Newtonian media: drag coefficient and wall effects. *Chemical Engineering and Processing*, 30(2), 61-67

Swamee, P.K., Ojha, C.S.P., 1991. Drag coefficient and fall velocity of non-spherical particles. *J. Hydraul. Eng.* 117, 660-667.

Turton R., Clark N.N., 1987. An explicit relationship to predict spherical particle terminal velocity *Powder Technology*, 53, 127-129